Exploiting the IRT-THESEUS Telescope to observe Quasars

Lindita Hamolli[1], Mimoza Hafizi[1], Francesco De Paolis[2] & Achille A. Nucita[2]

1- University of Tirana, Albania

2- University of Salento and INFN, Lecce, Italy

THESEUS CONFERENCE, VIRTUAL - 23-26 MARCH 2021

THESEUS Observatory

- Soft X-ray Imager (SXI, 0.3-5 keV)
- **Infrared Telescope (IRT, 0.7-1.8 μm)**
- X-Gamma rays Imaging Spectrometer (XGIS, 2 keV-20 MeV)

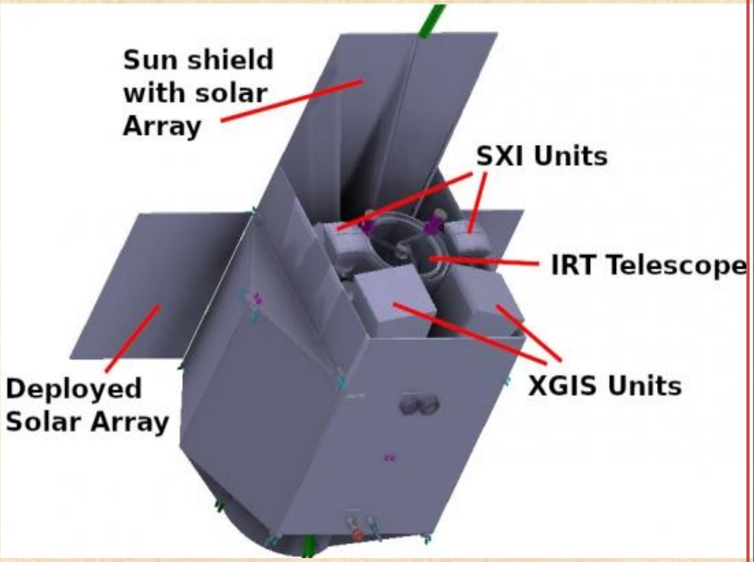

IRT-Telescope

- **How many Quasars would be observed by IRT-THESEUS**

  1. The AB mag (300s) is 20.6 for H band
  2. THESEUS will observe 64% of the sky

- **Lensed Quasars observed by IRT-THESEUS**

  1. IRT-THESEUS angular resolution is 1 arcsec

Quasars observed by IRT-THESEUS

The number of Quasars is calculated by the integration

$$N = \int_{z_1}^{z_2} \int_{L_{min}}^{L_{max}} \phi(L, z) dL dV_c$$

The Quasar luminosity function (QLF) is found by Lacy et al., in 2015, based on data of the Spitzer telescope: ϕ^*, γ^1 *and* γ^2 have fixed values, whereas:

$$\phi(L, z) = \frac{d\phi}{dlogL} = \frac{\phi^*}{\left[\left(\frac{L}{L^*}\right)^{\gamma_1} + \left(\frac{L}{L^*}\right)^{\gamma_2}\right]}$$

$$log_{10}L^*(z) = log_{10}L_0^* + k_1\epsilon + k_2\epsilon^2 + k_3\epsilon^3$$

$$\epsilon = log_{10}((z+1)/(z+z_{ref}))$$

$$dV_c = D_H \frac{(1+z)^2 D_A^2}{E(z)} d\Omega dz$$

$$D_H = \frac{c}{H_0}$$

$$E(z) = \sqrt{\Omega_m(1+z)^3 + \Omega_k(1+z)^2 + \Omega_\Lambda}$$

Test on Spitzer Space Telescope

- Band 3.6 *μm* with the apparent magnitude 18, Williams & Bonanos, 2016.

$$L_{\min} = L_{sun} 10^{\left(-17.88 - \log \frac{23.04\times10^{-24}}{D_L^2}\right)}$$

$$L_{sun} \doteq 3.83\times10^{33} \text{ erg/s} \qquad L_{max} = 10^{47} erg/s$$

- Number of Quasars observed by Spitzer in overall sky **N=2.55x10^{4}**

- Lacy & Sajina, in 2020, show that over 20,000 AGN candidates exist in the Spitzer archive.

- With its apparent magnitude, Spitzer could not observe Quasars with *z* higher than 2.58

$$\phi(L,z)$$

$$\log_{10}(\phi^*) = -4.75 \ Mpc^{-3}$$

$$\log_{10}(L_0^*) = 31.92 \ erg\, s^{-1}\, Hz^{-1}$$

$$z_{ref} = 2.5$$

$$\gamma_1 = 1.07 \qquad \gamma_2 = 2.48$$

$$k_1 = 1.05 \qquad k_2 = -4.71 \qquad k_3 = -0.034$$

$$dV_c$$

$$\Omega_m = 0.30 \qquad \Omega_k = 0 \qquad \Omega_\Lambda = 0.70$$

$$H_0 = 70 \ km\, s^{-1}\, Mpc^{-1}$$

Results on IRT-THESEUS

- The AB mag (300s) is 20.6 in H band (Amati et al. 2018). Using the Vega - AB Magnitude Conversion, we define the apparent magnitude to be 19.21

$$L_{\min} = L_{sun} 10^{\left(-18.396 - \log \frac{23.04 \times 10^{-24}}{D_L^2}\right)}$$

$$L_{max} = 10^{47} erg/s$$

- Number of Quasars observed by IRT-THESEUS in overall sky **N=3.35x10^5**

- Since, 64% of the sky will be monitored by IRT-THESEUS, it reduces to **N=2.14x10^5**

- With its apparent magnitude, IRT could not observe Quasars with *z* higher than 4.23

Gravitational Lensing

- A light ray from a distant source passes close to a mass distribution is bent. *General Relativity* (*Einstein, 1916*) predicted an angle 2x larger than Newtonian Gravity.

$$\alpha = \frac{4GM}{c^2\xi}.$$

- The lens equation is found to be (*Einstein, 1936*)

$$\theta - \beta = \theta_E^2/\theta.$$

$$\theta_E = \sqrt{\frac{4GM(\theta_E)}{c^2}\frac{D_{LS}}{D_S D_L}}$$

- D_S, D_L & D_{LS} are the angular diameter distances observer-source, observer-lens and lens-source.

$$D(z_1, z_2) = \frac{c}{H(z_1)}\frac{1+z_1}{1+z_2}\int_{z_1}^{z_2}\frac{dz'}{E(z')}$$

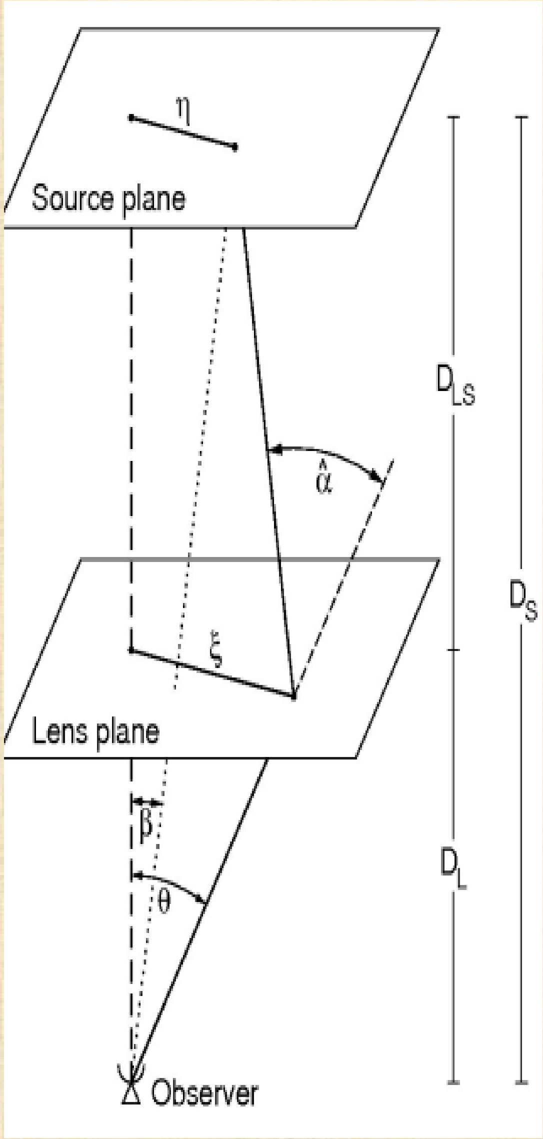

Three Classes of lensing

A) **Strong lensing.** High distortions, Einstein rings, arcs and multiple images separated by several arcsecs ***(Galaxy Cluster SDSS J1004+4112, HST).***

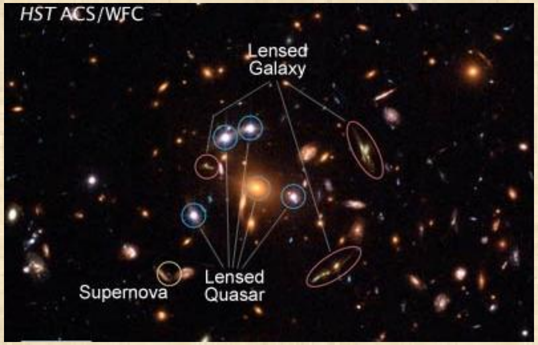

B) **Weak lensing**. Much smaller distortions due to large angular separations of the lensing galaxies or galaxy clusters to the line of sight (**"Topographical map" of the dark matter in the Bullet Cluster, detected using weak lensing, Miyazaki et al., 2015).**

A) **Microlensing**. No visible distortions, but a variable magnification of the source light (***Paczynski, 1986).*** Small mass lenses **($10^{-6}<M/M_S<10^3$).** The Einstein angular radius is of the order of the μarcsec.

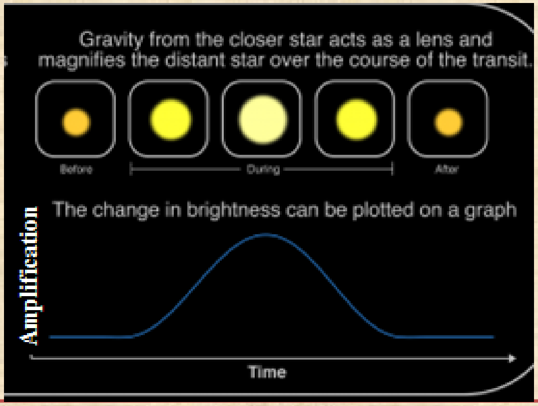

Quasar lensing

Quasar lensing is a strong lensing with double or quadruple images.

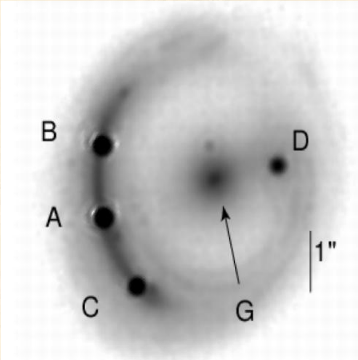

Fig 1. The four-image lens RXJ1131–1231. G is the galaxy. Z_Q=0.658 and Z_G=0.295

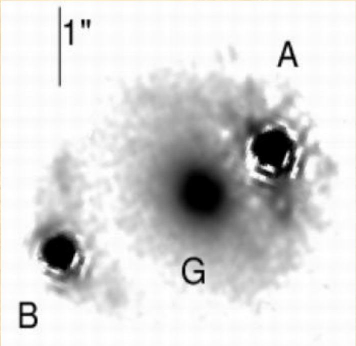

Fig 3. The two-image lens HE1104–1805. G is the lens galaxy and A and B are the quasar images, Z_Q=2.32

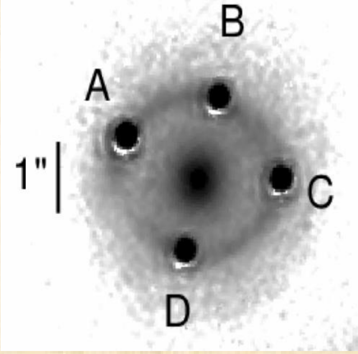

Fig 2. The four-image lens HE0435–1223. Z_Q=1.639 and Z_G=0.454

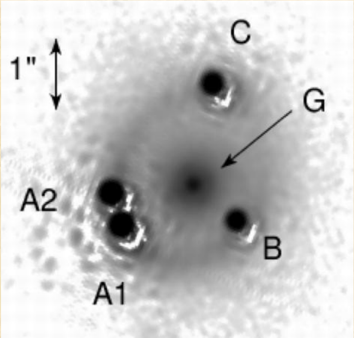

Fig 4. The four-image lens PG1115+080 G is the lens galaxy .

The algorithm of the Quasar lensing

- Generate the redshift of the quasar, following the corresponding distribution (slide 11);
- Generate the redshift of the galaxy, following the corresponding distributions (slide 12); Constrain that the galactic redshift be lower than the quasar redshift. The number of galaxies that fulfilling this condition for each Quasar is found by the cumulative number of galaxies ;
- For each generated galaxy, we extract its mass by the stellar mass function (slide 13) and based on the relation between the stellar mass of the galaxy and stellar velocity distribution (slide 14), find its velocity dispersion;
- Based on the Singular Isothermal Sphere model (SIS) for the galaxies, the galaxy and Quasar redshifts, we define the Einstein angle θ_E for the couple Quasar/galaxy ;
- Extract a uniformly distributed number **n** in the interval (0,1) and, considering 200 billions of galaxies in the Universe, keep the couple when $n<10^8 x \theta_E^2/14$ (aligned couple), otherwise reject it (nonaligned couple);
- Repeat the procedure for all expected quasars and keep the predicted aligned couples;
- For each aligned couple, comparing its Einstein angle with the resolution of the instrument, estimate the number of quasars expected to be observed by it.

Quasar redshift distribution

Quasar redshift distribution from SDSS Data Catalog (Third Data Release), Schneider et al. 2005.

It contains 46,420 quasars with spectroscopic redshifts from 0.08 to 5.41. The area covered by the catalog is ≈ 4188 deg^2.

A clear majority of quasars have redshifts below 2, the median redshift is 1.47, (the mode is 1.85). There are 520 quasars at redshifts greater than four, of which 17 are at redshifts greater than five.

The catalog contains 69 quasars with redshifts below 0.15.

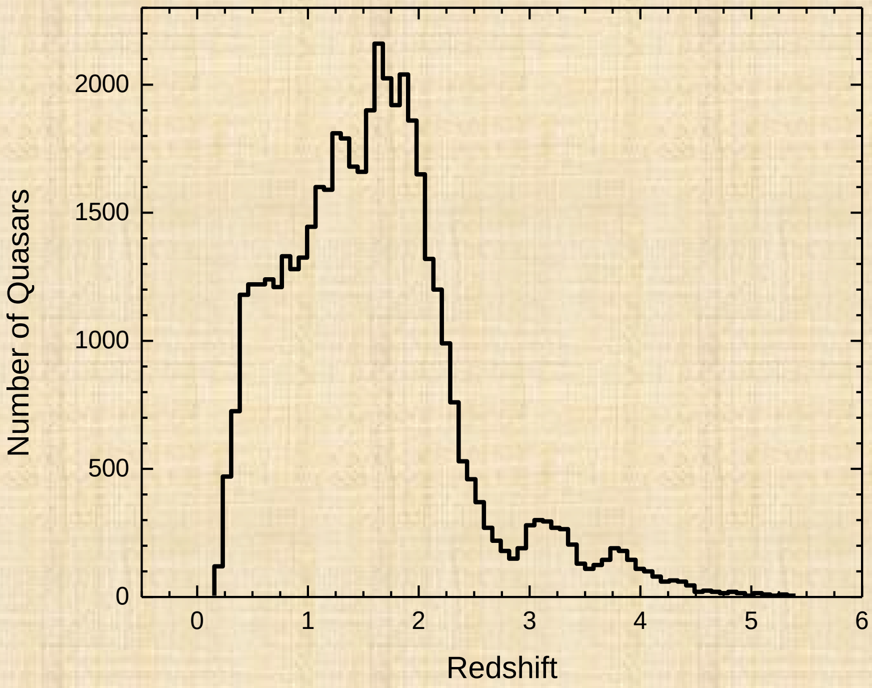

The redshift histogram of 46,420 quasars. The redshift bins have a width of 0.076. The dips at redshifts of 2.7 and 3.5 are caused by the lower efficiency of the selection algorithm at these redshifts, Schneider et al. 2005.

Galaxy redshift distribution

The photometric (checked also by spectroscopy) redshift distribution of 7,000 galaxies obtained by Appenzeller et al. 2004, through the analysis of distant galaxies observed near the South Galactic Pole by FORS Deep Field (ESO VLT), in a sky area of ≈ 7x7 arcmin^2.

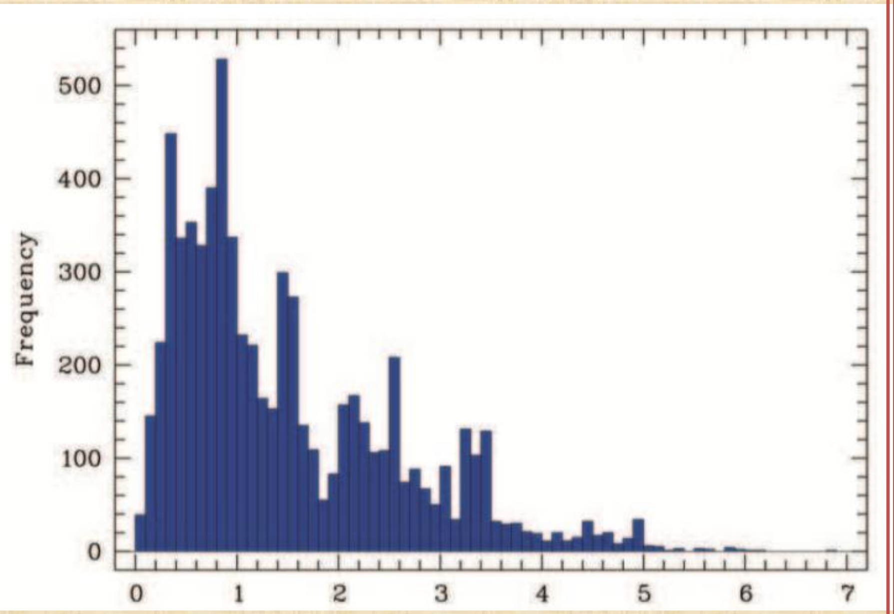

FDF histogram: The frequency is the number of galaxies within redshift intervals of 0.1. Conspicuous maxima at distinct redshifts (e.g. at z = 0.3, 0.8,2.4, and 3.4) reflect the local sponge-like large-scale structure of the matter distribution in the universe, *Appenzeller et al. 2004*.

- The number of galaxies with redshifts lower than z_Q of the quasar is found by the cumulative number of galaxies with $\mathbf{z<z_Q}$.

Galaxy mass distribution

The SMF (Stellar Mass Function) is described by a double (up to z=3) and a single (beyond that bin) Schechter function (Schechter 1976):

$$\Phi(M)dM = \left[\Phi_1^*\left(\frac{M}{M_*}\right)^{\alpha_1} + \Phi_2^*\left(\frac{M}{M_*}\right)^{\alpha_2}\right]\exp\left(-\frac{M}{M_*}\right)\frac{dM}{M_*}.$$

The parameters are estimated by Davidzon et al. 2017, best fitting the data of COSMOS2015 catalogue.

This catalogue includes ultra-deep photometry from UltraVISTA-DR2 (ESO), SPLASH (Spitzer), and Subaru/Hyper Suprime-Cam,

up to z ≈ 6.

redshift	$\log M_\star$ $[h_{70}^{-2}\,M_\odot]$	α_1	$\Phi_{\star1}$ $[10^{-3}\,h_{70}^3\,\mathrm{Mpc}^{-3}]$	α_2	$\Phi_{\star2}$ $[10^{-3}\,h_{70}^3\,\mathrm{Mpc}^{-3}]$
			Total sample		
$0.2 < z \leqslant 0.5$	$10.78^{+0.13}_{-0.14}$	$-1.38^{+0.08}_{-0.25}$	$1.187^{+0.633}_{-0.969}$	$-0.43^{+0.62}_{-0.60}$	$1.92^{+0.73}_{-0.78}$
$0.5 < z \leqslant 0.8$	$10.77^{+0.09}_{-0.08}$	$-1.36^{+0.05}_{-0.06}$	$1.070^{+0.287}_{-0.315}$	$0.03^{+0.43}_{-0.43}$	$1.68^{+0.33}_{-0.33}$
$0.8 < z \leqslant 1.1$	$10.56^{+0.05}_{-0.05}$	$-1.31^{+0.05}_{-0.06}$	$1.428^{+0.306}_{-0.308}$	$0.51^{+0.35}_{-0.34}$	$2.19^{+0.40}_{-0.41}$
$1.1 < z \leqslant 1.5$	$10.62^{+0.08}_{-0.07}$	$-1.28^{+0.05}_{-0.05}$	$1.069^{+0.222}_{-0.240}$	$0.29^{+0.40}_{-0.42}$	$1.21^{+0.23}_{-0.22}$
$1.5 < z \leqslant 2.0$	$10.51^{+0.08}_{-0.07}$	$-1.28^{+0.06}_{-0.06}$	$0.969^{+0.202}_{-0.208}$	$0.82^{+0.48}_{-0.52}$	$0.64^{+0.18}_{-0.17}$
$2.0 < z \leqslant 2.5$	$10.60^{+0.15}_{-0.12}$	$-1.57^{+0.12}_{-0.21}$	$0.295^{+0.173}_{-0.177}$	$0.07^{+0.70}_{-0.74}$	$0.45^{+0.12}_{-0.12}$
$2.5 < z \leqslant 3.0$	$10.59^{+0.36}_{-0.36}$	$-1.67^{+0.26}_{-0.26}$	$0.228^{+0.300}_{-0.300}$	$-0.08^{+1.73}_{-1.73}$	$0.21^{+0.14}_{-0.38}$
$3.0 < z \leqslant 3.5$	$10.83^{+0.15}_{-0.15}$	$-1.76^{+0.13}_{-0.11}$	$0.090^{+0.064}_{-0.039}$		
$3.5 < z \leqslant 4.5$	$11.10^{+0.21}_{-0.21}$	$-1.98^{+0.14}_{-0.13}$	$0.016^{+0.020}_{-0.009}$		
$4.5 < z \leqslant 5.5$	$11.30^{+1.22}_{-1.22}$	$-2.11^{+0.34}_{-0.22}$	$0.003^{+0.002}_{-0.002}$		

Galactic velocity dispersion

Analyzing the SDSS and SHELS data, Zahid et al. 2016, proposed a relation between the stellar velocity dispersion (*σ)* and the stellar mass (*M)* of the galaxies, which is a power law with a break point,

$$\begin{cases} \sigma(M) = \sigma_b \left(\frac{M}{M_b}\right)^{\alpha_1} & for \quad M \leq M_b \\ \\ \sigma(M) = \sigma_b \left(\frac{M}{M_b}\right)^{\alpha_2} & for \quad M > M_b. \end{cases}$$

$$\rightarrow$$

$log(M_b/M_\odot) = 10.26,$

$log(\sigma_b) = 2.073,$

$\alpha_1 = 0.403$ $\alpha_2 = 0.293$

The Singular Isothermal Distribution

As the model of galaxies we assume a Singular Isothermal Sphere (SIS) distribution. This spherical mass distribution yields flat rotation curves, such as are observed for spiral galaxies. Their density distribution is described by Schneider et al. 2006.

$$\rho(r) = \frac{\sigma^2}{2\pi G r^2}.$$

By projecting this density along the line of sight, we obtain the surface density and the mass of the lens inside a radius *R* from the galactic center in the galactic plane is given by

$$\Sigma(\xi) = 2\frac{\sigma^2}{2\pi G}\int_0^\infty \frac{dz}{\xi^2 + z^2} = \frac{\sigma^2}{2G\xi}$$

$$M(R) = \int_0^R 2\pi\xi\Sigma(\xi)d\xi = \frac{\pi}{G}\sigma^2 R$$

by replacing it in lens equation, we obtain

$$\theta_E = 4\pi(\frac{\sigma}{c})^2\frac{D_{LS}}{D_S}$$

Testing the Code. SDSS

Testing through observational results of SDSS:

- Inada et al. 2012, selected a sample of **50,836** quasars in the Sloan Digital Sky Survey (SDSS) Data, with the redshift range of $0.6 < z < 2.2$, and found **26 lensed quasars** brighter than i=19.1 with image separations **from 1″ < θ < 20″.**

- We generate similar conditions and obtain 33 synthetic lensed quasars.
- Small excess of low z Quasars and a similar excess of high z Quasars.

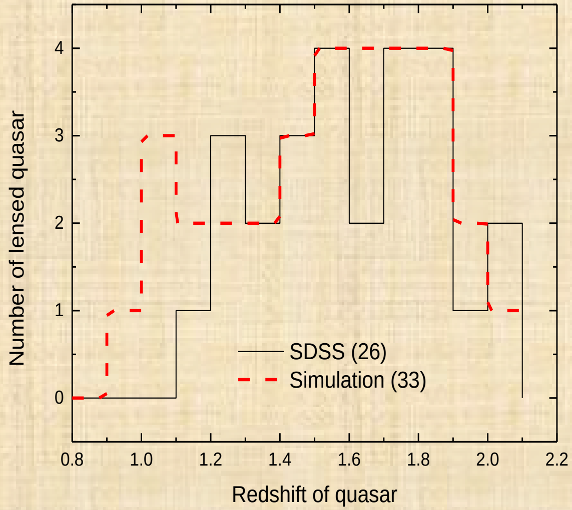

Histogram of redshift distributions for 26 observed and 33 synthetic lensed quasars in the case of SDSS (Hamolli, Hafizi).

Lensed Quasars by IRT-THESEUS

- Based on the IRT angular resolution of 1 arcsec, Amati et al. 2018 and the fraction of sky that it will observe (64%), we find about 140 Quasars to be lensed by a foreground galaxy.

Conclusions-Discussion

- The number of Quasars that could be observed by the IRT-THESEUS is $N=2.14\times10^5$.

- From the observed Quasars by IRT-Theseus, about 140 Quasars will to be lensed by a foreground galaxy.

Our results are based to QLF obtain by the Lacy et al. 2015, even if the spectral bands are slightly different (0.7 – 1.8 μm instead 5 μm).

Thank you!

- Lacy et al., 2015, Apj. 802(2):102
- Lacy & Sajina 2020, *Nature Astronomy*, 4(4):352–363,
- Einstein, A. 1916, AnP, 354,769
- Miyazaki et al., 2015, ApJ, 807, 22
- Einstein A., 1936, Science, 84, 506
- Schneider et al., 2005, AJ, 130, 367
- Appenzeller et al., 2004, Msngr, 116, 18
- Paczynski B., 1986, 304, 1
- Davidzon et al., 2017, A&A, 605, 70
- Zahid et al., 2016, ApJ, 832(2):203
- Nayyeri et al., 2017, ApJS, 228, 7
- Hasinger et al., 2005, A&A , 441, 417
- Walton et al., 2015, ApJ, 805, 161
- Evans et al., 2010, ApJS, 189, 37
- Amati et al., 2018, AdSpR, 62, 191
- Inada et al., 2012 AJ, 143, 119